ARTICLE

A Mutation in *CCDC50,* a Gene Encoding an Effector of Epidermal Growth Factor–Mediated Cell Signaling, Causes Progressive Hearing Loss

Silvia Modamio-Høybjør, Ángeles Mencía, Richard Goodyear, Ignacio del Castillo, Guy Richardson, Felipe Moreno, and Miguel Ángel Moreno-Pelayo

We previously mapped a novel autosomal dominant deafness locus, *DFNA44,* by studying a family with postlingual, progressive, nonsyndromic hearing loss. We report here on the identification of a mutation in *CCDC50* as the cause of hearing loss in the family. *CCDC50* encodes Ymer, an effector of epidermal growth factor (EGF)–mediated cell signaling that is ubiquitously expressed in different organs and has been suggested to inhibit down-regulation of the EGF receptor. We have examined its expression pattern in mouse inner ear. Western blotting and cell transfection results indicate that Ymer is a soluble, cytoplasmic protein, and immunostaining shows that Ymer is expressed in a complex spatiotemporal pattern during inner ear development. In adult inner ear, the expression of Ymer is restricted to the pillar cells of the cochlea, the stria vascularis, and the vestibular sensory epithelia, where it shows spatial overlap with the microtubule-based cytoskeleton. In dividing cells, Ymer colocalizes with microtubules of the mitotic apparatus. We suggest that *DFNA44* hearing loss may result from a time-dependent disorganization of the microtubule-based cytoskeleton in the pillar cells and stria vascularis of the adult auditory system.

Nonsyndromic hearing impairment, with hearing loss as the sole clinical symptom, is a very common inherited sensory disorder characterized by a vast genetic heterogeneity. Mutations in >100 genes are predicted to be associated with this sensory deficit in humans. At present, 99 loci for nonsyndromic hearing loss have been mapped, and 42 of the responsible genes have been identified (Hereditary Hearing Loss Home Page). The genes currently identified encode a variety of proteins with different functional roles in the auditory system.[1–3] This repertoire will presumably increase, given the complexity of the hearing process and the large number of loci that have been mapped but for which the responsible gene remains to be identified.

Recently, we mapped a novel autosomal dominant deafness locus (*DFNA44* [MIM 607453]) in a Spanish family segregating progressive, postlingual, nonsyndromic sensorineural hearing loss. The hearing loss in this family is initially moderate and affects mainly low to mid frequencies (125–2,000 Hz). Later, it progresses to involve all the frequencies (a flat audiometric profile) and leads to a profound hearing loss by the 6th decade. The onset of the hearing loss occurs in the 1st decade of life (ages 6–10 years). No evidence of either vestibular dysfunction or tinnitus has been reported in the patients with *DFNA44* hearing loss. In addition, CT rules out inner ear malformations as the cause of deafness.[4] *DFNA44* maps to chromosome 3q28–29 within a 3-cM critical interval defined by markers *D3S1314* and *D3S2418.* Sequence analysis excluded *CLDN16* (MIM 603959), *FGF12* (MIM 601513), and *IL1RAP* (MIM 602626) as genes responsible for *DFNA44* hearing loss. A novel gene, *CCDC50,* (UniGene Hs.478682)[5] was subsequently positioned in the interval. This gene is ubiquitously expressed and encodes Ymer, a protein recently identified as an effector of epidermal growth factor (EGF)–mediated cell signaling.[6,7] Another UniGene for *CCDC50* (Hs.592514) locates 3′ to Hs.478682 in the *DFNA44* interval. Hs.592514 comprises 222 ESTs, 4 of which are cochlear (accession numbers AW020156.1, H88039.1, H88255.1, and BI491203.1 [Morton Cochlear EST Database]). It appears to constitute an alternate 3′ end for *CCDC50,* since a Gnomon program analysis generates two hidden Markov models (hmm556752 and hmm556986) that result in a more extended 3′ UTR region. Consequently, we considered *CCDC50* a putative candidate gene for *DFNA44* hearing loss, given that it is expressed in cochlea. The human gene (UniGene Hs.478682) is organized in 12 exons, and two alternative transcripts have been identified thus far. The longer transcript (GenBank accession number NM_178335) contains a 1,449-nt ORF encoding a protein of 482 aa, whereas a shorter variant (GenBank accession number NM_174908) without exon 6 encodes a protein of 305 aa and is predominant in all the organs tested.[5] Ymer does not show significant similarity with any described protein. The predicted amino acid sequence for Ymer does not indicate the presence

From the Unidad de Genética Molecular, Hospital Ramón y Cajal, Madrid (S.M.-H.; A.M.; I.d.C.; F.M.; M.A.M.-P.).; and School of Life Sciences, University of Sussex, Brighton, United Kingdom (R.G.; G.R.)

Received November 22, 2006; accepted for publication March 16, 2007; electronically published April 24, 2007.

Address for correspondence and reprints: Dr. Miguel Ángel Moreno-Pelayo, Unidad de Genética Molecular, Hospital Ramón y Cajal, Carretera de Colmenar Km 9, 28034 Madrid, Spain. E-mail: mmoreno.hrc@salud.madrid.org

Am. J. Hum. Genet. 2007;80:1076–1089. 0002-9297/2007/8006-0008$15.00
DOI: 10.1086/518311

of transmembrane domains or a signal peptide, although a coiled-coil domain is encoded by exons 3 and 4, and two motifs interacting with ubiquitin (MIUs) are encoded by exons 7 and 8 (MIU1) and by exons 8 and 9 (MIU2).[8] Residues encoded by exon 5 undergo posttranslational modification. Lysine 129 is ubiquitinated, and tyrosines 145 and 146 are phosphorylated in response to EGF stimulation. Ymer may inhibit down-regulation of the EGF receptor (EGFR).[9–11] At present, however, most aspects of Ymer function are still poorly characterized.

We report here on the identification of *CCDC50* as the gene responsible for *DFNA44* hearing loss in the Spanish family. We have also established the spatiotemporal expression pattern of Ymer in the mouse inner ear and have investigated its subcellular localization. On the basis of these results, we discuss the roles it may play during development and functional maturation of the inner ear.

Material and Methods

The protocols of this study were approved by the institutional review board of Hospital Ramón y Cajal (Madrid).

Mutation Screening of the Human CCDC50 *Gene*

Primers to PCR amplify all the exons and intron-exon boundaries of the human *CCDC50* gene were designed using Oligo 4.0 (Molecular Biology Insights). PCRs were performed in standard conditions, as described elsewhere.[12] PCR products were purified with the QIAquick PCR purification kit (Qiagen) and were directly sequenced using the BigDye Terminator v3.1 Cycle Sequencing Ready Reaction Kit in an ABI PRISM 3100 genetic analyzer (Applied Biosystems). To isolate the c.1394_1401dupCACGGCAT mutation, the exon 11 amplimer obtained from patient III:1 (fig. 1) was cloned into pUC19 (New England Biolabs), was transformed into XL1-Blue competent cells, and was grown on Luria Bertani plates with isopropyl-β-D-thiogalactopyranoside and X-gal under ampicillin selection. Plasmid DNA obtained from several white colonies was sequenced using pUC (-47) and pUC (-48) universal primers. Mutant sequences contained a CACGGCAT 8-bp tandem duplication. For the detection of the mutation in the human population, we developed a size-based screening test in which exon 11 is amplified with a pair of primers, one of which is fluorescently labeled. Allele size was obtained after capillary electrophoresis in an ABI PRISM 3100 genetic analyzer (Applied Biosystems), by analysis with the GeneScan program (Applied Biosystems). The wild-type allele is 8 bp smaller than that of the mutant.

RT-PCR Analysis for Transcript Variants of the Murine Ccdc50 *Gene*

Total RNA was prepared from the mouse cochleae at embryonic day (E) 18.5, postnatal day (P) 0, and P14 and from mouse lung, brain, and liver at P58, and the contaminating genomic DNA was eliminated using RNase-free DNase treatment. Approximately 1 μg of total RNA was reverse transcribed using SuperScriptase II (Invitrogen) and oligo-dT primer. The sequences of primers used to RT-PCR amplify the different transcripts of the mouse *Ccdc50* gene are as follows: F1, 5′-CCATGGCCGACGTGAGTG-3′; F5, 5′-TCTTTGTACCCATGTCATGAAGAAAA-3′; F6, 5′-ATTGCAAGAAGAAGAACTTTTGGAA-3′; F7, 5′-CGTGAGTGTAGATCAGTCCAAGTTG-3′; F8, 5′-CCATGTCATGAAGAAAATAATCTCTTG-3′; F10, 5′-CGCGGGGAGGTATTTCTGAG-3′; R1, 5′-CCAGAATGGCACACAGAAGGAC-3′; R2, 5′-GCCGATCCCTTTTTGTTTGTATT-3′; R4, 5′-AGGCTGTTTGTTCTTTAATTTTGAG-3′; R8, 5′-CAAGAGATTATTTTCTTCATGACATGG-3′; R9, 5′- CATTAGAAGTCGAGCAATTTCCAA-3′; and R14, 5′-CCATGGTGATGAGACTGCTTTTC-3′. Table 1 summarizes the primer pairs used in the amplification of the different *Ccdc50* transcript variants. Primary RT-PCRs were performed in a thermocycler (Perkin-Elmer 9700) with the use of 0.75 U of FastStart Taq polymerase (Roche Applied Science) and 1:50 of the cDNA preparation in a final volume of 15 μl; 40 cycles (at 96°C for 30 s, 58°C for 30 s, and 72°C for 1 min/kb) were used. Secondary amplifications were done using nested primers (see table 1) and 1.5 μl of a 1:100 dilution of the previous PCR (F1-R4); 30 cycles (at 96°C for 30 s, 63°C for 15 s, and 72°C for 30 s) were used. Direct sequencing of PCR products was performed following the standard procedure described above. RACE (rapid amplification of cDNA ends) analyses were performed on total RNA from E17.5 whole-embryo mouse, with use of the Marathon cDNA Amplification kit (BD Biosciences-Clontech).

Northern Blot Analysis

Northern analysis was performed on a commercial blot (FirstChoice Mouse Blot I [Ambion]) containing mRNA from 10 different mouse tissues (heart, brain, liver, spleen, kidney, embryo, lung, thymus, testes, and ovary), in accordance with the manufacturer's instructions. Mouse *Ccdc50* ORF cDNA (transcript 1) was amplified with the F1-R1 primer pair, was cloned into pGEM-5Zf(+) (Promega), and was linearized. Antisense transcripts were generated using T7 polymerase (Strip-EZ RNA probe synthesis [Ambion]) and were nonisotopically labeled (BrightStar Psoralen-Biotin [Ambion]). The northern blot was hybridized overnight at 60°C with the full-length antisense mouse *Ccdc50* probe and was washed at 58°C three times at low stringency and two times at high stringency. Nonisotopic detection was performed according to the manufacturer's directions (BrightStar Biodetect [Ambion]). The blot was stripped and reprobed with antisense probe generated from pTRI-β-actin mouse control template (Ambion).

Antibodies and Immunoblot Analysis

Immune serum against two nonoverlapping synthetic peptides based on the predicted sequence of the mouse Ymer protein located in the N-terminal (peptide I, RIQEKKDEDIARLL) and C-terminal (peptide II, NQHSTTWHLPKSES) regions of the protein (see fig. 2) were raised in rabbit (CovalAb). After three boosts of immunization, the antiserum was affinity purified. The specificity of the polyclonal antibody was tested by immunoblotting of protein extracts prepared from the inner ear. In brief, cochleae from P2 mice were homogenized and sequentially extracted with Tris-buffered saline (TBS) (150 mM NaCl and 10 mM Tris-HCl [pH 7.4]), high-salt solution (1.0 M NaCl and 10 mM Tris-HCl [pH 7.4]), low-salt solution (10 mM Tris-HCl [pH 7.4]), and 1% nonionic detergent (1% Triton X-100 and 10 mM Tris-HCl [pH 7.4]). High-speed centrifugation after each extraction was used to produce soluble supernatants from which the protein was precipitated with trichloroacetic acid or acetone before gel electrophoresis. The insoluble fraction remaining after centrifugation in TX-100 solution was solubilized in SDS-PAGE sample buffer. Protein

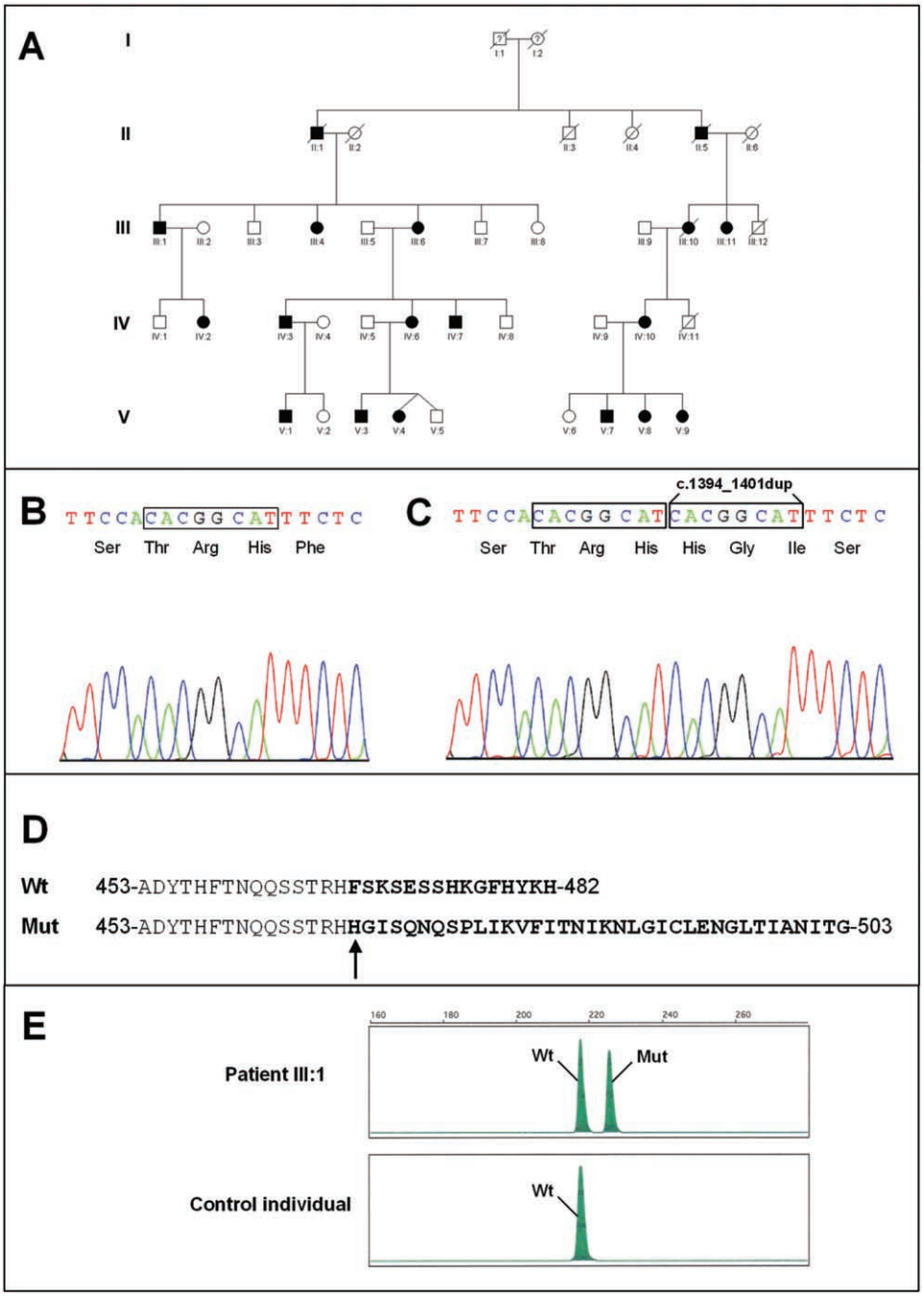

Figure 1. Mutation analysis of *CCDC50*. *A,* Pedigree of the family with *DFNA44* hearing loss. Square symbols represent males; circles represent females. Black symbols represent hearing-impaired subjects; white symbols represent individuals with normal hearing. A question mark inside a symbol indicates that the clinical status of the subject is unknown. Individuals V:4 and V:5 are DZ twins. *B* and *C,* Fragment of *CCDC50* exon 11 from patient III:1 showing the presence of two alleles, wild type and mutant, respectively, after being cloned separately into the pUC19 vector. The eight nucleotides that are duplicated in the mutant allele are boxed. *D,* Alignment of the C-terminal fragment of the deduced Ymer protein for both wild-type (wt) and mutant (mut) alleles. Arrow points to the site where the frameshift takes place, and amino acids that are different in the two alleles are shown in bold. *E,* Diagnostic test for the c.1394_1401dupCACGGCAT mutation, based on the separation of wild-type and mutant alleles with the use of an automated genetic analyzer.

Table 1. Primer Pairs Used in the Amplification of the Different Mouse *Ccdc50* Transcript Variants

Transcript Variant and PCR	Primary PCR		Nested PCR	
	Forward	Reverse	Forward	Reverse
1:				
1	F1	R4	…	…
2:				
1	F1	R4	F7	R9
2	F1	R4	F6	R2
3:				
1	F1	R4	F7	R8
2	F1	R4	F5	R2
4:				
1	F1	R4	F7	R8
2	F1	R4	F8	R9
3	F1	R4	F6	R2
5:				
1	F1	R4	F7	R14
2	F1	R4	F10	R2
6:				
1	F1	R4	F7	R14
2	F1	R4	F10	R9
3	F1	R4	F6	R2
7:				
1	F1	R4	F7	R8
2	F1	R4	F8	R14
3	F1	R4	F10	R2
8:				
1	F1	R4	F7	R8
2	F1	R4	F8	R14
3	F1	R4	F10	R9
4	F1	R4	F6	R2

samples were run under reducing conditions on 10% polyacrylamide gels and were transferred to a polyvinylidene fluoride Hybond-P membrane (Amersham Biosciences). Membranes were blocked for 1 h with 3% semiskimmed milk in TBS Tween (TBST) (150 mM NaCl, 10 mM Tris-HCl [pH 7.2], and 0.05% Tween 20) and were incubated overnight with the primary antibody at 1:400 dilution. After three washes with TBST, the membrane was incubated with alkaline phosphatase–conjugated goat anti-rabbit secondary antibody (DAKO) at 1:1,000 dilution, and the bound antibodies were visualized with nitro-blue tetrazolium chloride/5-bromo-4-chloro-3′ indolyl phosphate p-toluidine solution.

Transfections

NIH-3T3 and Hela cells were grown in Dulbecco's modified Eagle medium (Sigma) containing 10% fetal bovine serum, 1% glutamine, and 1% penicillin/streptomycin under standard conditions, were transiently transfected with JetPEI (Qbiogene), and were processed for immunofluorescence as reported elsewhere.[13] For transfection purposes, mouse *Ccdc50* transcripts 1 and 2 were PCR amplified (forward primer, 5′-CCATGGCCGACGTGAGTG-3′; reverse primer, 5′-CCAGAATGGCACACAGAAGGAC-3′) with the use of mouse brain cDNA as a template and were cloned into the dicistronic expression vector pIRES-hrGFP-1a (Stratagene), which is driven by the cytomegalovirus promoter. Similarly, human *CCDC50* transcripts 1 and 2 were amplified with the forward 5′-CGGGCTCCGGATATTTGGTA-3′ and reverse 5′-TGAGTCCATTTTCAAGGCAGATTC-3′ primers with the use of cDNA from Epstein-Barr virus–transformed human B lymphocytes and were cloned into the expression vector pIRES-hrGFP-1a (Stratagene), and the 8-bp duplication was introduced at exon 11 by mutagenesis (Quick Change Site-Directed Mutagenesis Kit [Stratagene]).

Immunohistochemistry

Mouse inner ears were dissected and fixed in 3.7% formaldehyde in 0.1 M sodium phosphate buffer (pH 7.4). Tissues obtained from P5 mice onwards were decalcified with 0.5 M EDTA (pH 8.0) for 5 d before sectioning. Inner ears were cryoprotected in 30% sucrose in PBS, were embedded in 1% low-gelling agarose in 18% sucrose in PBS, and the agar blocks were mounted for cryosectioning onto microtome chucks with use of optimal cutting temperature compound (Tissue Tek [Miles Scientific]). Sections were cut in a cryotome at −30°C.

For immunostaining, cryosections were blocked with 10% horse serum in TBS containing 1 mM sodium azide for 1 h and were incubated overnight with 1:100 dilution of the primary antibody. After three TBS washes, the slides were incubated with a 1:100 dilution of the fluorescein isothiocyanate (FITC)–conjugated swine anti-rabbit secondary antibody (DAKO) for 1 h. Sections were mounted in Vectashield H-1000 (Vector Laboratories). Staining specificity was confirmed by substituting the primary antibody with nonimmune rabbit immunoglobulin G (IgG) at the same concentration or by preabsorbing antibodies with the two peptide antigens. Preimmune sera from the rabbit used to generate the polyclonal anti-Ymer antibody was also used to check specificity. Tissue-section slides were visualized in an Axioplan 2 fluorescence microscope (Carl Zeiss), and the images were captured with a Spot-Junior Camera (Diagnostic Instruments).

For colocalization experiments, the following primary antibodies were used: mouse monoclonal antibodies to α-tubulin (A-11126 [Molecular Probes] and TU-16 [Abcam]), acetylated α-tubulin (clone 6–11B-1 [Sigma]), polyglutamylated tubulin (T9822 [Sigma]), and β-tubulin I and II (clone JDR.3B8 [Sigma]). Primary antibodies were detected with Alexa Fluor 594-conjugated goat anti-rabbit IgG (H+L) (Molecular Probes) and FITC-conjugated goat anti-mouse $F(ab')_2$ IgG fragment (Sigma). Actin was detected with rhodamine or Alexa-Fluor 350–conjugated phalloidin. For colocalization studies, whole-mount and single-cell preparations were analyzed on a Zeiss LSM510 laser scanning confocal microscope.

Results

Identification of the Mutation in CCDC50 *Causing* DFNA44 *Hearing Loss*

Sequence analysis of all exons and flanking intronic sequences of *CCDC50* in the affected subject III:1 (fig. 1*A*) revealed eight sequence variations (table 2). Seven of these changes, located in exons 3, 6, 7, and 10, included four silent changes and three nonsynonymous amino acid substitutions that, with the exception of the synonymous change at exon 3, corresponded to previously reported nonpathogenic SNPs. The remaining change corresponded to a heterozygous mutation in exon 11 (c.1394_1401dupCACGGCAT, with respect to the longer transcript [GenBank accession number NM_178335]). This

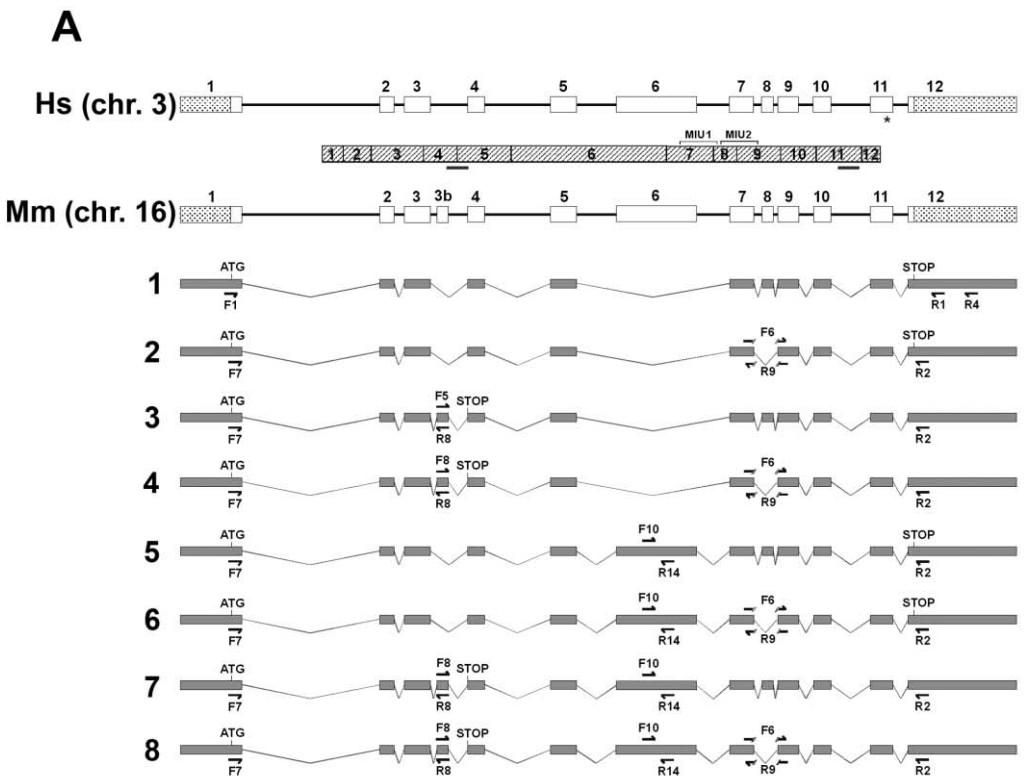

B

```
ttcaatttagTCTTTGTACCCATGTCATGAAGAAAATAATCTCTTGTCTTCTGACTgtaagtttgt
```

C

```
ctccactcagACCAGTCAAGGTCAAGGAGGGACAGGGAACTGGGTTCTGGACACTCAAAGTTTTGTAGAC
TCCAAAACGATGGGAAGACTGTAAGGCAGAAGGAGAAACCAAGGCATCAACAGAAGAACTTGGAAGATCT
GGAAGAACACCACCCATCAGAGAGGTCCCTGCCTTCTGCTAGCTGGGGCAGAGGGAGGGATGGTGCCCAG
ACTGCCTGTGAGCAGCAGGAAAGAAAGCGATCTGGTCAGGAGAGGCTCTGGAAATCTCCACTTCCGAAGA
TCCGCGGGGAGGTATTTCTGAGCATTGACTCTGAAGACTGGGAAGCTGACTGGAGCTCTGGAACCCGGAG
TCCAGAAAAGCAGTCTCATCACCATGGCAGACTTTCACCCAAGTCTTCACAGAAAACAGGACTTCCCTGT
AAGGAAATTGTATATGGGCGGGACCTTGGGCAAGGTGACCACAGAGAAAGGAGACATAGGCCCAGGACTT
CTCCCTTCTCAGAAGATAAAGAACTTCGCCACCACCATGTTGCAGgtaatgggtt
```

D

```
Hs intron 3     gtcaacttctctgaatttatttccttacccataacatgcggataataatctct
Mm exon 3b      --------------------TCTTTGTACCCATGTCATGAAGAAAATAATCTCT
                                    * *   *******  ****  ** **********

Hs intron 3     gtcccctctgcctcatagtttctttgggggatc
Mm exon 3b      -TGTCTTCTGACT--------------------
                 *  * **** **
```

Figure 2. Analysis of *Ccdc50* transcripts in the mouse inner ear. *A,* Schematic drawing of human (Hs) and mouse (Mm) *Ccdc50* genomic organization. Exons are represented by rectangles. The ORF is depicted in white, and the UTRs are dotted. The asterisk marks the site where the mutation was found in the family with *DFNA44* hearing loss. A diagram of the Ymer protein (*striped*) includes the position of the two MIU domains and the peptides in the N- and C-terminal regions (*gray bars*) used for generating the polyclonal antibody. Below, the eight *Ccdc50* transcript variants detected in mouse inner ear cDNA are shown. Primers used to amplify each variant are represented by arrows (see the "Materials and Methods" section). Primers F6 and R9 were designed to anneal with exons 7 and 9 (only the three most 3′ bases of each one are capable of annealing with exon 9 or 7, respectively), and thus they were used to amplify transcripts without exon 8. Primers F5, F8, and R8 were designed to anneal with exon 3b, and they were used to amplify transcripts that contain this exon. Primers F10 and R14 are specific to exon 6. *B* and *C,* Sequences of mouse *Ccdc50* exon 3b and exon 6, respectively. Intronic sequences are in lowercase letters. *D,* ClustalW alignment between human (Hs) *CCDC50* intron 3 and mouse (Mm) *Ccdc50* exon 3b.

Table 2. Sequence Variations Found in the ORF of the Human *CCDC50* Gene of Patient III:1

Exon and Sequence Variation[a]	State	Protein Level (Deduced)	dbSNP Identification Number
3:			
c.228C→T	Heterozygous	p.Arg76Arg	Not described
6:			
c.651T→C	Homozygous	p.His217His	*rs2028572*
c.678A→G	Heterozygous	p.Lys226Lys	*rs2028573*
c.773T→A	Homozygous	p.Ile258Asn	*rs2028574*
c.908A→G	Homozygous	p.Lys303Arg	*rs4677728*
7:			
c.995T→C	Homozygous	p.Met332Thr	*rs293813*
10:			
c.1269C→A	Homozygous	p.Ser423Ser	*rs364519*
11:			
c.1394_1401dup	Heterozygous	**p.Phe468HisfsX37**	…

NOTE.—All variations, except c.678A→G (exon 6) and c.1394_1401dup (exon 11), were also present in the individual with normal hearing, III:8, who did not inherit the disease chromosome. The pathogenic mutation is displayed in bold.

[a] Changes refer to the cDNA of the long isoform (RefSeq number NM_178335), position +1 corresponding to the A of the ATG initiation codon.

8-bp tandem duplication leads to a frameshift that replaces the last 15 aa of the protein by a novel 36-aa sequence (p.Phe468HisfsX37) (fig. 1*B*–1*D*). We took advantage of the size difference between the wild-type and mutant alleles to design a screening test to detect this mutation (see fig. 1*E* and the "Material and Methods" section). This test showed that the mutation segregated with the hearing impairment in the family. In addition, it was not present in 100 unrelated Spanish individuals with normal hearing. These findings indicate that c.1394_1401dupCACGGCAT is the pathogenic mutation responsible for *DFNA44* hearing loss in the family. We screened for this mutation in probands from 280 unrelated Spanish families displaying nonsyndromic sensorineural hearing loss. Of these patients, 135 belonged to families segregating autosomal dominant hearing impairment, and the remainder belonged to families in which the pattern of inheritance could not be defined unambiguously. The mutation was not detected in any of these probands.

Identification of Ccdc50 *Transcripts in the Mouse Inner Ear*

The orthologous mouse *Ccdc50* gene (UniGene Mm.258985) is also predicted to encode two isoforms. Transcript 1 (GenBank accession number NM_026202.2)[5] lacks exon 6 and corresponds to the shorter human variant. It is expressed in several tissues including the organ of Corti (GenBank accession number BQ567072.1) and is predicted to encode a protein of 305 aa. Transcript 2 (GenBank accession number NM_001025615.1), generated by exon 8 skipping, is expressed in the testis of the adult mouse (GenBank accession number AK016827.1) and is predicted to encode a protein of 290 aa (fig. 2*A*). *Ccdc50* is widely expressed in most tissues tested, but there is little information available concerning the different transcripts that are present in these tissues and their expression at the different stages of mouse inner ear development. We therefore performed RT-PCR analysis on mRNA from the mouse cochlea at E18.5, P0, and P14. This analysis detected the presence of transcripts 1 and 2 at all three developmental stages (fig. 3*A* and 3*B*). In addition, we used 5′-RACE-PCR to investigate the presence of putative novel exons upstream of the described *Ccdc50* exon 1 (data not shown). Although no other exons were found toward the 5′ region of the gene, sequence analysis of the 5′-RACE-PCR products revealed the existence of a novel exon between exons 3 and 4. This novel coding sequence, exon 3b, comprises a 46-bp sequence located 243 bp downstream of exon 3 in the genomic sequence (fig. 2*B*). A set of specific primers was therefore designed to amplify overlapping fragments of the full-length *Ccdc50* coding sequence and to investigate the presence of putative novel transcripts expressed in the inner ear containing this novel exon (see the "Material and Methods" section, figs. 2*A* and 3*A*, and table 1). This analysis led us to characterize two additional transcripts (transcripts 3 and 4) that are derived, respectively, from transcripts 1 and 2 by the inclusion of exon 3b. The presence of this exon in both transcripts leads to a frameshift that generates a premature stop codon at the beginning of exon 4. Transcripts including exon 3b are predicted to generate a shorter protein isoform of 95 aa. The last 15 aa of this isoform would correspond to the predicted protein fragment encoded by exon 3b. Similar to transcripts 1 and 2, the variants 3 and 4 were identified in the inner ear at all three stages tested (fig. 3*A*).

Although a BLAST analysis (BLASTN, TBLASTN, BLASTX, or cross-species megaBLAST performed against the Human Genome Database) did not reveal the existence of this exon in humans, a ClustalW alignment performed between the human *CCDC50* intron 3 and the mouse *Ccdc50*

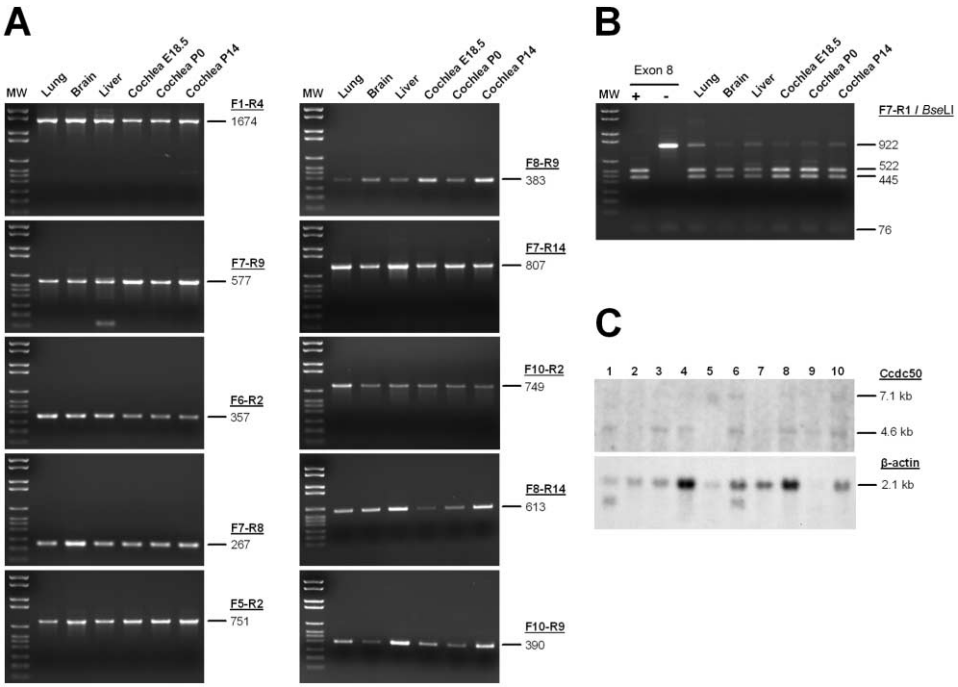

Figure 3. *A,* Panels showing the different RT-PCR amplification products of the overlapping fragments used to identify the different transcripts. Primer pairs and expected fragment sizes (in bp) are shown on the right. The first panel (F1-R4) represents the primary PCR, from which the remaining ones were obtained as nested PCRs. Each amplimer was confirmed by direct sequencing. *B,* Restriction pattern of the F7-R1 amplimer (nested PCR from F1-R4 containing the entire *Ccdc50* ORF) digested with *Bse*LI, showing the presence of transcripts 1 and 2. Restriction pattern of transcript 1 (with exon 8) includes three bands of 522 bp, 445 bp, and 76 bp. Transcript 2 (without exon 8) digestion yields two bands of 922 bp and 76 bp. Exon 8 positive and negative controls were obtained by amplifying cloned transcripts 1 and 2, respectively (see the "Material and Methods" section). *C,* Northern blot showing the expression pattern of *Ccdc50* in different mouse tissues. A probe against β-actin was used as a positive control. Lanes: 1, heart; 2, brain; 3, liver; 4, spleen; 5, kidney; 6, embryo; 7, lung; 8, thymus; 9, testes; and 10, ovary. MW = molecular-weight marker.

exon 3b sequences detected a stretch of human sequence with ~71% similarity to mouse exon 3b (fig. 2*D*). Conserved donor and acceptor splice sites, however, were not present, suggesting that it is unlikely that there are human splice variants containing the orthologous exon 3b. Further studies at the RNA level are necessary for a more definitive conclusion.

Although the mouse gene was not reported to contain an exon homologous to human exon 6, cross-species megaBLAST analysis, with the use of human exon 6 as a query, revealed a putative mouse exon 6, and the conceptual translation was ~60% identical to the human protein (hmm192144). We therefore designed mouse exon 6–specific primers (F10 and R14), and different RT-PCRs were performed. This strategy allowed us to identify up to four novel transcripts that include this exon (figs. 2*A* and 3*A* and table 1). The presence of exon 6 in these transcripts was confirmed by direct sequencing of different overlapping fragments (fig. 2*C*). RT-PCR analysis of lung, brain, and liver mRNA from a P58 mouse indicates that the expression of none of these transcripts, variants 1–8, is restricted to the mouse inner ear.

Analysis of a northern blot with mRNA from 10 different tissues (see the "Material and Methods" section) detected two bands of ~4.6 and 7.1 kb (fig. 3*C*). These findings indicated that the gene is ubiquitously expressed. The band sizes do not correspond with the expected length for mouse transcripts 1 and 2, reported to be ~3.5 kb. They are much longer and may correspond to transcripts with alternate 3′ ends. Indeed, the 7.1-kb band is similar to the predicted sizes of hmm192700 and hmm192422 (models for transcripts 1 and 2, respectively), which contain a 3′ UTR of up to 6 kb.

A processed *Ccdc50* pseudogene showing a 93% similarity with mouse transcript 1 is present on mouse chromosome 4 (GenBank accession number NG_005190.2). The expression of the pseudogene has not been reported so far, and it has a premature stop codon at exon 5. The specific amplification of *Ccdc50* gene transcripts was ensured by designing RT-PCR primer pairs that take into account the sequence variations that exist with respect to the pseudogene, and the PCR products were also verified by direct sequencing.

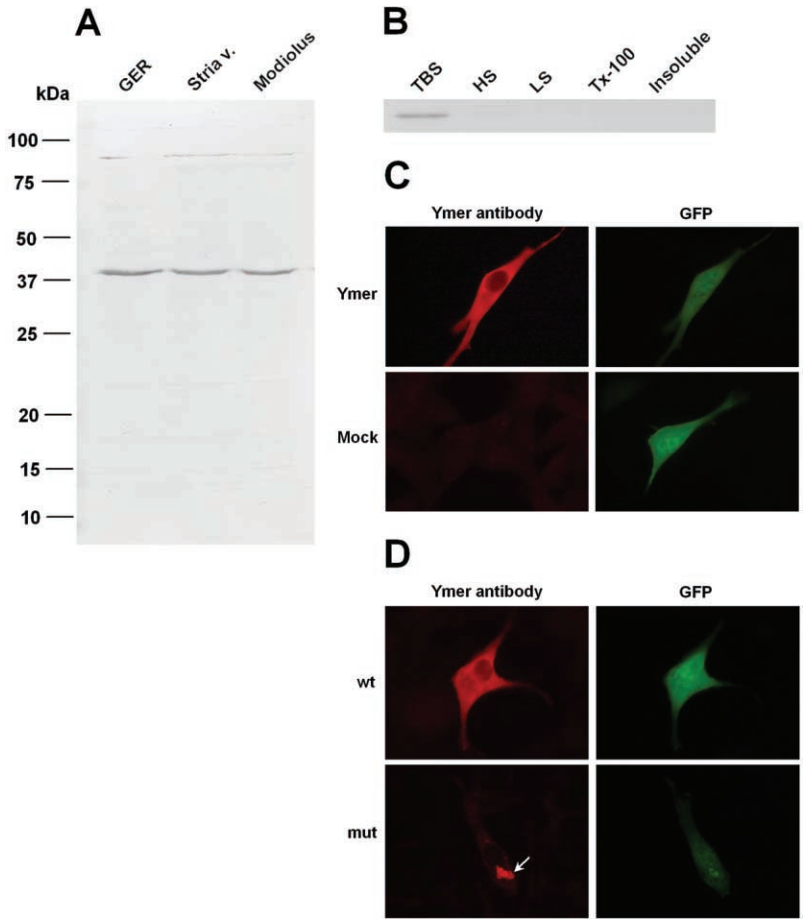

Figure 4. Western blot analysis and subcellular localization of the Ymer protein. *A,* Western blots of tissue samples from the GER, stria vascularis (stria v.), and modiolus of the mouse cochlea. A prominent band of ~38 kDa was revealed in the three tissues tested. A minor higher-mass band of ~88 kDa is also revealed and may correspond to a nonreducible dimeric form of the protein. *B,* Western blot performed on proteins prepared by sequentially extracting whole cochlear tissue in TBS, 1 M NaCl (high salt [HS]), 10 mM Tris (low salt [LS]), and 1% Triton X-100 (Tx-100). The residual remaining protein is the insoluble fraction. Ymer is detected only in the TBS soluble fraction. *C,* Subcellular localization of mouse Ymer protein in transiently transfected NIH-3T3 cells. Cells transfected with the mouse *Ccdc50* transcript 1 show a cytoplasmic distribution of Ymer protein (*red*) that is absent from the nucleus (*top left*). Similar results were obtained in Hela cells or when both types of cells were transfected with transcript 2 (data not shown). No staining was obtained in cells transfected with the empty vector (mock [*bottom left*]). The transfection level was visualized by GFP expression (*right, top and bottom*). *D,* NIH-3T3 cells transfected with the human mutated transcript 1 showed an aggregated perinuclear distribution of the protein (*arrow*). Similar results were obtained in cells transfected with the mutated human transcript 2.

Ymer Is a Soluble Cytoplasmic Protein

A polyclonal antibody to Ymer was raised by injecting a rabbit simultaneously with two peptides based on the predicted sequence of the mouse protein, one located in the N-terminal half of the protein (residues 103–116) and the other in the C-terminal region (residues 283–296) (see the "Materials and Methods" section and fig. 2*A*). The antibody was affinity purified on a column to which both peptides had been conjugated, and its specificity was assessed by western blot analysis of protein extracts prepared from three different tissues of the P2 mouse inner ear: the greater epithelial ridge (GER), the stria vascularis, and the modiolus. This analysis revealed a single prominent band of ~38 kDa in all three tissues. This molecular mass is similar to that predicted from murine Ymer isoforms 1 and 2 (fig. 4*A*). A minor band of approximately double the mass was also detected and may correspond to a stable dimeric form of the protein. These two bands were not observed when blots were probed with nonimmune rabbit IgGs at the same concentration (data not shown), indicating the specificity of the purified antibody. On the basis of the location of the two peptides used to generate the polyclonal antibody, it should be possible to detect the predicted isoforms 5 and 6 (fig. 2*A*). They have not been detected, however, which suggests they are expressed at levels that escape the sensitivity of this technique.

The solubility of the Ymer protein was estimated by immunoblotting proteins prepared by sequentially ex-

tracting cochlear tissues with normal saline, buffers of high and low ionic strength, and a buffer containing nonionic detergent (see the "Material and Methods" section). The 38-kDa band was readily extracted in TBS (fig. 4*B*). The subcellular localization of Ymer was investigated in NIH-3T3 and Hela cells transiently transfected with the murine wild-type transcripts 1 and 2. Transfected cells showed that Ymer is globally distributed in the cytoplasm and is not present in the nucleus (fig. 4*C*). Staining was not observed in nondividing cells transfected with the empty (mock) vector. Collectively, these results indicate that Ymer is likely to be a soluble cytoplasmic protein.

To evaluate whether the identified mutation alters the subcellular distribution of the protein, NIH-3T3 and Hela cells were transiently transfected with mutated human transcripts 1 and 2. Mutated protein is expressed but, unlike the wild-type protein, is restricted to the perinuclear area (fig. 4*D*).

Expression Pattern of the Ymer Protein in the Mouse Inner Ear

The spatiotemporal expression pattern of the Ymer protein was investigated in the developing and adult mouse inner ear by immunohistochemistry with the affinity-purified antibody. We compared Ymer expression in the mouse inner ear at embryonic stages E14.5 and E17.5 and at several postnatal stages from P2 to P69.

At E14.5, strong punctate immunostaining was detected in the otic mesenchyme. Moreover, expression was detected in the cells lining the lumen of the primitive cochlear duct and in the nerve fibers of the spiral ganglion (fig. 5*A*). Immunolabeling of nerve fibers invading the cochlear epithelium was also observed at this stage. At E17.5, a strong signal was detected only in the mesenchyme around the cochlear duct (fig. 5*B*).

By P2, the mesenchymal staining became weaker, except in the region of the spiral limbus, and Ymer expression was observed for the first time in the apical region of the developing pillar cells (PCs). Staining was also observed in the cytoplasm of the outer hair cells (OHCs), in their innervating nerve fibers, and in the marginal cells of the stria vascularis at this stage (fig. 5*C*). At P9 and P12, Ymer was detected strongly through the entire length of the inner and outer PCs, and the staining in tissues of mesenchymal origin was restricted to two major structures, the spiral limbus and the spiral ligament. Also at P9 and P12, labeling became more evident in the stria vascularis (fig. 5*D* and 5*E*). By P14 and P16, strong staining was still evident in the PCs and in the marginal cells of the stria vascularis. Staining was weak in the spiral limbus and spiral ligament at this stage and had begun to appear in Deiter's cells (fig. 5*F* and 5*G*). At P19 and P22, staining was still intense in the PCs and stria vascularis and was strong in the cell bodies and the processes of Deiter's cells. Weaker staining was observed in the spiral limbus and spiral ligament at these stages (fig. 5*H* and 5*I*). At P31, when the inner ear is functionally mature, Ymer was expressed only in the stria vascularis and PCs (fig. 5*J*). At P69, the staining was still strong in PCs and less intense in stria vascularis (fig. 5*K*).

At all stages, for negative controls, we substituted the primary antibody with nonimmune rabbit IgGs at the same concentration or used preimmune sera from the rabbit used to generate the polyclonal antibody. Similar results were obtained in both controls, with nonspecific staining only in one region of the cochlea corresponding to the cells of the spiral ligament in the later stages of development (fig. 5*L*). These results indicate that the cochlear localization and expression levels of Ymer vary dynamically with time from embryonic stages onward (table 3).

The expression of Ymer in the vestibular maculae and the cristae ampullaris was similar to that observed in the cochlea (fig. 6)—that is, with a strong signal observed in the mesenchyme at the initial embryonic stages that progressively became weaker and was less prominent in the adult (P33). Staining of the nerve fibers innervating the sensory epithelia was seen at E17.5 and P2 (fig. 6*A*–6*C*). Staining was initially detected in some cells of the vestibular epithelium at E17.5 and became more evident at P2 (fig. 6*B*–6*D*). Later, the staining increased and persisted to adult stages in which it was mainly restricted to the apical cytoplasm of the epithelial cells (fig. 6*E* and 6*F*).

Ymer Colocalizes with Microtubules of the Cytoskeleton and Mitotic Apparatus

The staining pattern of Ymer through the entire length of PCs and Deiter's cells suggested this protein could be associated with their prominent microtubule-based cytoskeleton. This possibility was investigated by double immunolabeling for Ymer and different types of tubulins in postnatal mouse inner ear sections. This analysis showed that Ymer exhibits overlap with the microtubule bundles of PCs and Deiter's cells and with the complex microtubule structure in the interdigitating processes of the marginal and intermediate cells in the stria vascularis (fig. 7*A* and 7*C*). Moreover, a clear colocalization was observed in the apical cytoplasm of vestibular epithelial cells (fig. 7*B*). The subcellular localization of Ymer was similarly investigated in the mouse NIH-3T3 cell line. Double labeling of nontransfected cells revealed that Ymer colocalized with microtubules of the mitotic apparatus of cells undergoing division. During the nuclear division, or karyokinesis, Ymer colocalizes with microtubules of the mitotic spindle. In the final steps of cell division, during cytokinesis, Ymer overlaps with the midzone, a region of bundled microtubules between the migrated chromosomes, and then with the microtubule midbody contained in the intercellular bridge that is created as the cleavage furrow ingresses and compresses the midzone (fig. 7*D*). Taken together, these results suggest that Ymer is associated with microtubule-based structures.

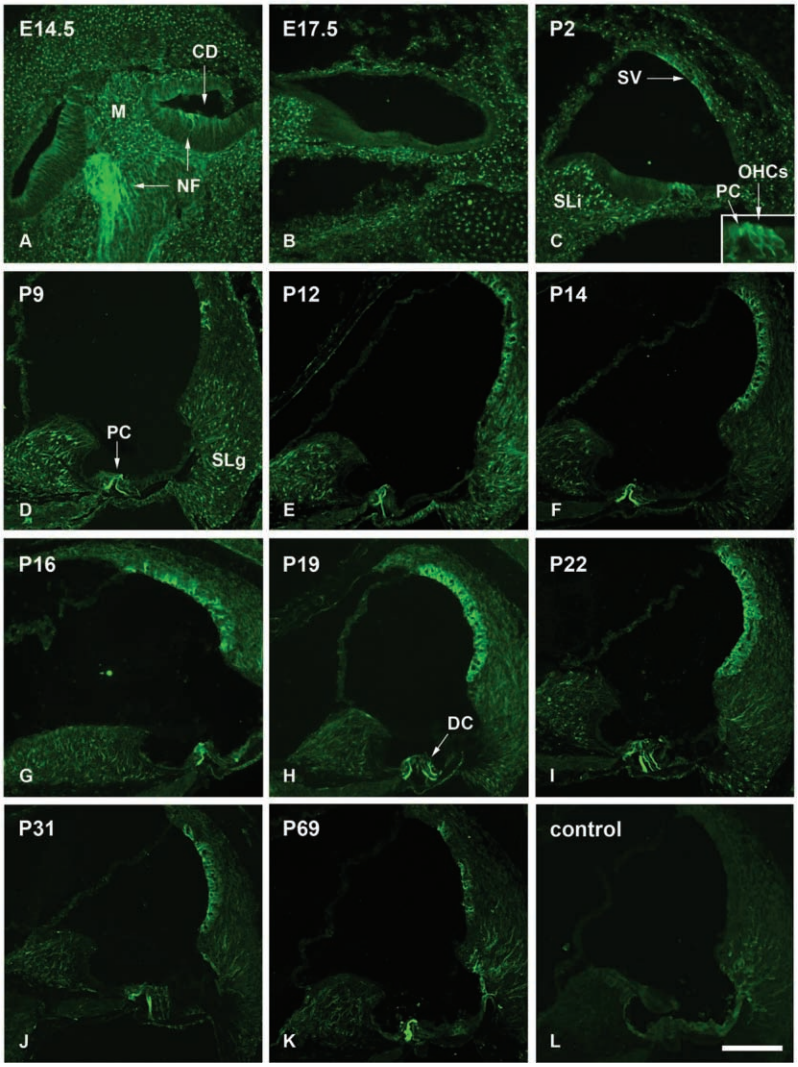

Figure 5. Spatiotemporal expression pattern of Ymer protein in the mouse cochlea. Immunohistochemistry was performed on mouse inner ear sections at embryonic stages E14.5 and E17.5 and several postnatal stages from P2 to P69. Inset in panel C shows a magnification of the apical region of developing PCs and the OHCs. Panel L shows a negative control performed on a P69 section with the use of nonimmune rabbit IgG. Similar results were obtained when we used preimmune sera from the rabbit used to generate the polyclonal antibody. M = mesenchyme; CD = cochlear duct; NF = nerve fibers; SLi = spiral limbus; SV = stria vascularis; SLg = spiral ligament; DC = Deiter's cells. Scale bar = 100 μm.

Discussion

The results of this study indicate that a mutation in *CCDC50,* a gene encoding a tyrosine phosphorylated effector of EGF-mediated cell signaling known as "Ymer," causes nonsyndromic, postlingual, progressive sensorineural *DFNA44* hearing loss in the Spanish family. A thorough investigation of the protein expression pattern in the mouse inner ear reveals that a spatiotemporal correlation can be established between the distribution of Ymer and the tubulin cytoskeleton during the development and postnatal maturation of different cell types in the organ of Corti.[14,15] At E14.5, Ymer was detected in the nerve fibers of the spiral ganglion. Tubulin is one of the major components of the cells of the spiral ganglion and their axonal projections during development.[14] In OHCs, Ymer is detected at P2 as cells elaborate their microtubule cytoskeleton and begin to express specific properties as motor cells.[14–17] Ymer is initially present in the apex of PCs at ~P0, at a time and place where the nucleation of microtubules begins,[18] and then throughout the whole PC body as the cells acquire their adult morphology and the microtubule scaffold projects toward the basal membrane to eventually span the entire length of the cell.[19] In Deiter's cells, which mature after PCs,[14,16] Ymer is clearly observed at P19. Interestingly, colocalization studies show spatial overlap between Ymer and the microtubule cytoskeleton in PCs and Deiter's cells, and the staining pattern

is compatible with the structure of the compact sheaths seen in these cell types.[20,21] In the stria vascularis, which starts its maturation after birth,[22] Ymer is first detected at P2. It is known that a complex rearrangement of microtubules occurs during maturation of marginal and intermediate cells of the mouse stria vascularis.[23,24] Interestingly, in the adult stria, a clear colocalization of Ymer is seen with the microtubule-based cytoskeleton. Of note, although Ymer is dynamically expressed during inner ear development, its expression in the adult cochlea appears to be restricted to the PCs and the stria vascularis. A similar correlation is observed during the maturation of the vestibular system. At E17.5, the expression of Ymer is observed in the nerve fibers of the vestibular sensory epithelium, and, in the adult, it colocalizes with the microtubule-based cytoskeleton that is prominent in the apical cytoplasm of vestibular hair cells.[25] Notably, Ymer colocalizes with microtubules of the mitotic apparatus in cells undergoing division (fig. 7*D*), suggesting it is also functioning in processes that involve the dynamic rearrangement of microtubules. However, the existence of the breast cancer cell line MCF7, in which Ymer is not expressed,[11,26] suggests that Ymer is not involved in the crucial steps of mitosis.

Collectively, these findings strongly suggest that Ymer is associated with microtubule-based structures and that it may play roles in the developing and adult inner ear. It can therefore be suggested that the pathogenesis of *DFNA44* hearing loss, a postlingual, progressive form of deafness, results from the destabilization of the cytoskeleton in the PCs and stria vascularis of the adult cochlea. PCs are supporting cells with a highly developed cytoskeleton composed of microfilaments and microtubules, which undergoes a mechanical stress in response to the sound stimuli. Moreover, the distribution and orientation of microtubules in marginal and intermediate cells is crucial to maintain the architecture of the stria vascularis,[23,27] and it has been suggested that the depolymerization of microtubules in marginal cells of the adult mouse may underlie strial atrophy.[24] Thus, a failure in the integrity of the cytoskeleton over time may explain the progressive hearing loss. Finally, the fact that Ymer is expressed at similar levels in PCs and stria vascularis in the basal and apical turns (data not shown) may explain why all frequencies are affected in the patients. Interestingly, although *CCDC50* is ubiquitously expressed, the hearing loss in this family is not accompanied by alterations in other organs. Several examples exist of genes with widespread expression patterns and a role in inner ear development that, once mutated, cause a hearing loss with clinical features similar to those observed in our family with *DFNA44* hearing loss. This is the case for *EYA4,* a gene encoding a transcriptional activator that is involved in *DFNA10* (MIM 601316) hearing impairment,[28] and for *TFCP2L3*, a gene encoding a transcription factor responsible for *DFNA28* (MIM 608641) hearing loss.[29] The existence of redundancy is one of the possible mechanisms

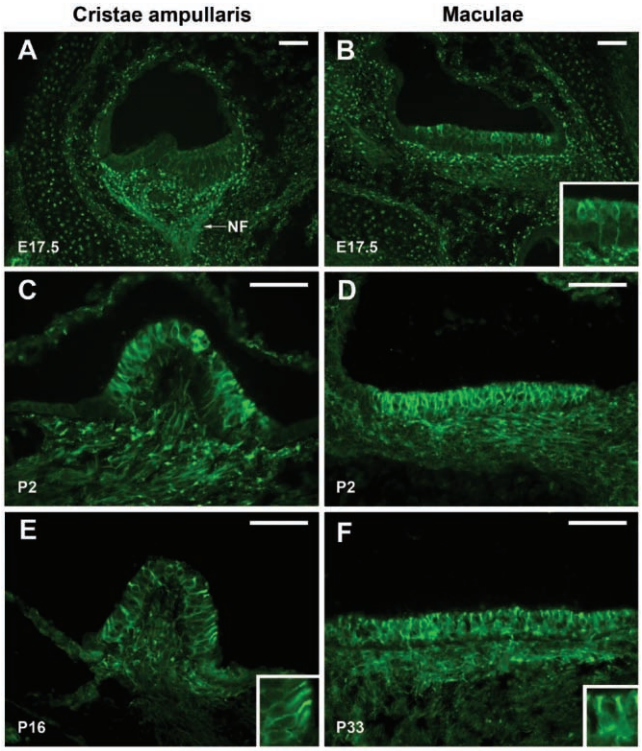

Figure 6. Spatiotemporal expression pattern of Ymer protein in the mouse vestibular system. Ymer staining was investigated on vestibular sections from embryonic (*A* and *B,* E17.5), neonatal (*C* and *D,* P2) and adult (*E,* P16 and *F,* P33) stages. Panels A, C, and E show cristae ampullaris; panels B, D, and F show maculae (*B* and *F,* utricles; *D,* saccule). Insets in panels B, E, and F show magnifications of the corresponding sensory epithelia. NF = nerve fibers. Scale bars = 50 μm.

Table 3. Expression Level of Ymer Protein in Different Mouse Cochlear Structures at Different Stages of Development

	Stage										
Structure	E14.5	E17.5	P2	P9	P12	P14	P16	P19	P22	P31	P69
Mesenchyme and derived structures	++++	++++	++++	+++	+++	++	+	+	+	−	−
Nerve fibers	++++	−	−	−	−	−	−	−	−	−	−
OHCs	−	−	+++	−	−	−	−	−	−	−	−
PCs	−	−	+	++++	++++	++++	++++	++++	++++	++++	++++
Deiter's cells	−	−	−	−	−	+	+	++++	++++	+	−
Stria vascularis	−	−	++	++	+++	+++	+++	++++	++++	+++	++

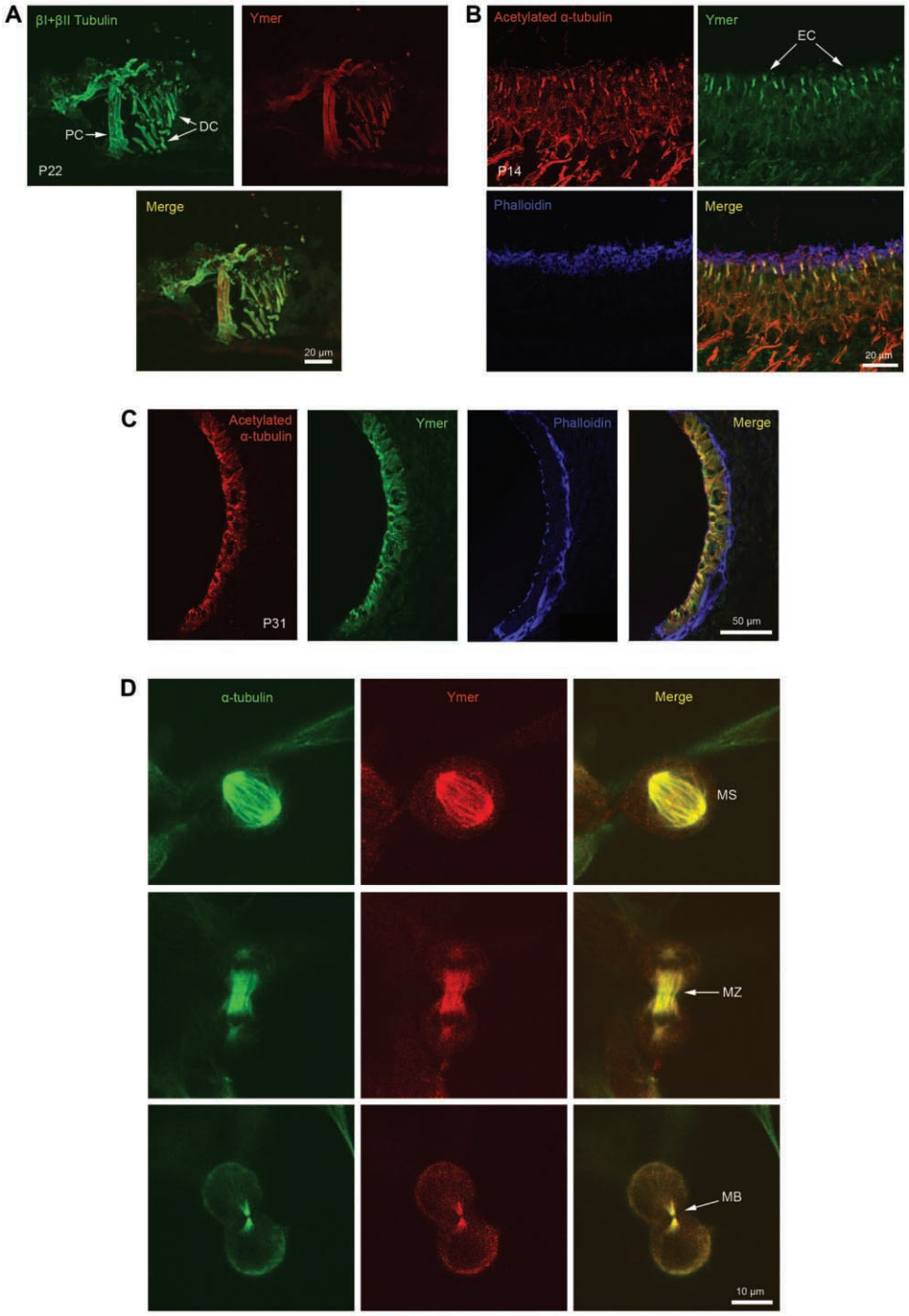

Figure 7. Colocalization studies of Ymer and different tubulins in inner ear sections and NIH-3T3 cells. *A,* In the mature cochlea (P22), Ymer colocalizes with ($\beta1+\beta2$) tubulin in the cytoskeleton of PCs and Deiter's cells (DC). Similar results were obtained for α-tubulin and for both acetylated and polyglutamylated tubulin (data not shown). *B,* In the utricule of a P14 mouse, Ymer shows spatial overlap with the cytoskeleton of microtubules in the apical cytoplasm of the epithelial cells (EC). *C,* In adult stria vascularis (P31), Ymer colocalizes with the microtubule-based cytoskeleton of marginal and intermediate cells. In panels B and C, no colocalization is seen with the actin cytoskeleton (phalloidin panel). *D,* Ymer colocalizes with microtubules of the mitotic apparatus in nontransfected NIH-3T3 cells that are undergoing cell division. In metaphase (*top panels*), Ymer distribution overlaps with microtubules of the mitotic spindle (MS). During early telophase (*middle panels*), Ymer colocalizes with the midzone (MZ), a region of bundled microtubules between the migrated chromosomes. In late telophase (*lower panels*), as the cleavage furrow ingresses compressing the midzone, Ymer colocalizes with the microtubule midbody (MB) contained in the intercellular bridge.

that may explain the nonsyndromic nature of these phenotypes.

Several studies have demonstrated that EGF[30–33] and platelet-derived growth factor (PDGF)[34,35] are required for the development and differentiation of the inner ear. The cellular response to these growth factors is mediated by their corresponding receptors, EGFR and PDGFR, and by the phosphorylation of a large number of intracellular effector molecules.[36–38] Currently, little is known about the precise role that Ymer plays in the EGF-mediated signaling pathway. It has been reported that human Ymer undergoes tyrosine phosphorylation and ubiquitination in response to EGF stimulation and that it may be an inhibitor of EGFR downregulation.[9–11] In this process, the modified shorter isoform binds to the ubiquitinated EGFR through residues that involve the phosphorylation sites and MIU domains.[11] The longer isoform (with exon 6) does not, however, bind to the EGFR and has no effect on its downregulation.[11] As for the longer human isoform, the predicted mouse isoform 2, which lacks several residues shared by both MIU domains as a consequence of exon 8 skipping, may not be involved in EGFR regulation. In addition, mouse transcripts 3, 4, 7, and 8 are predicted to generate a shorter isoform of 95 aa that would lack all the described EGFR binding domains and the motifs for posttranslational modifications. Interestingly, a recombinant shorter isoform of human Ymer that lacks the C-terminal portion in which the *DFNA44* mutation was found still retains the ability to interact with EGFR,[11] thus suggesting that the mutation identified in this work might not be affecting Ymer's role on EGFR regulation. Transfection experiments performed with the mutated human isoforms 1 and 2 show, however, that the mutant protein is mislocalized and accumulates in the perinuclear area, suggesting that the mutation identified in the family with *DFNA44* hearing loss might cause a loss of function of the Ymer protein. Further investigation is required to isolate the distinct roles that Ymer isoforms are predicted to play. In summary, the results obtained in this work provide interesting clues that may improve our understanding of the role for Ymer, particularly in hearing and deafness.

Acknowledgments

We thank members of the Spanish family, whose participation made this study possible. We also express our gratitude to I. Varela, F. Setien, and S. Tenbaum, for kindly donating tissue and cDNA from different mouse organs; to A. Perez-Rosado, for providing the NIH-3T3 and Hela cells; and to D. Weil, for advice in antibody generation. S.M.H. was the recipient of fellowships from Spanish Ministerio de Ciencia y Tecnología and European Molecular Biology Organization. A.M.R was the recipient of a fellowship from Fondo de Investigaciones Sanitarias. This work was supported by Spanish Ministerio de Ciencia y Tecnología grant SAF2005–06355, Programa Ramón y Cajal (to I.d.C.), Spanish Fondo de Investigaciones Sanitarias grants FIS G03/203, PI-051942, and CP03/00014, European Commission FP6 Integrated Project EUROHEAR grant LSHG-CT-2004–512063, and the Wellcome Trust.

Web Resources

Accession numbers and URLs for data presented herein are as follows:

BLAST, http://www.ncbi.nlm.nih.gov/BLAST/
ClustalW, http://www.ebi.ac.uk/clustalw
dbSNP, http://www.ncbi.nlm.nih.gov/SNP/
GenBank, http://www.ncbi.nlm.nih.gov/GenBank/ (for *CCDC50* transcripts 1 [accession number NM_174908] and 2 [accession number NM_178335], *Ccdc50* transcripts 1 [accession number NM_026202.2] and 2 [accession number NM_001025615.1]), mouse organ of Corti [accession number BQ567072.1] and adult mouse testis [accession number AK016827.1] *Ccdc50* ESTs, and *Ccdc50* pseudogene [accession number NG_005190.2])
Hereditary Hearing Loss Homepage, http://webhost.ua.ac.be/hhh/
Morton Cochlear EST Database, http://www.brighamandwomens.org/bwh_hearing/human-cochlear-ests.aspx (for cochlear ESTs [accession numbers AW020156.1, H88039.1, H88255.1, and BI491203.1])
Online Mendelian Inheritance in Man (OMIM), http://www.ncbi.nlm.nih.gov/Omim/ (for *DFNA44, CLDN16, FGF12, IL1RAP, DFNA10,* and *DFNA28*)
UniGene, http://www.ncbi.nlm.nih.gov/UniGene/ (for *CCDC50* sequences [accession numbers Hs.592514 and Hs.478682] and *Ccdc50* [accession number Mm.258985])

References

1. Petersen MB (2002) Non-syndromic autosomal-dominant deafness. Clin Genet 62:1–13
2. Friedman TB, Griffith AJ (2003) Human nonsyndromic sensorineural deafness. Annu Rev Genomics Hum Genet 4:341–412
3. Petersen MB, Willems PJ (2006) Non-syndromic, autosomal-recessive deafness. Clin Genet 69:371–392
4. Modamio-Høybjør S, Moreno-Pelayo MA, Mencia A, del Castillo I, Chardenoux S, Morais D, Lathrop M, Petit C, Moreno F (2003) A novel locus for autosomal dominant nonsyndromic hearing loss (DFNA44) maps to chromosome 3q28–29. Hum Genet 112:24–28
5. Vazza G, Picelli S, Bozzato A, Mostacciuolo ML (2003) Identification and characterization of C3orf6, a new conserved human gene mapping to chromosome 3q28. Gene 314:113–120
6. Blagoev B, Ong SE, Kratchmarova I, Mann M (2004) Temporal analysis of phosphotyrosine-dependent signalling networks by quantitative proteomics. Nat Biotechnol 22:1139–1145
7. Kratchmarova I, Blagoev B, Haack-Sorensen M, Kassem M, Mann M (2005) Mechanism of divergent growth factor effects in mesenchymal stem cell differentiation. Science 308:1472–1477
8. Penengo L, Mapelli M, Murachelli AG, Confalonieri S, Magri L, Musacchio A, Di Fiore PP, Polo S, Schneider TR (2006) Crystal structure of the ubiquitin binding domains of rabex-5 reveals two modes of interaction with ubiquitin. Cell 124:1183–1195
9. Zhang Y, Wolf-Yadlin A, Ross PL, Pappin DJ, Rush J, Lauffenburger DA, White FM (2005) Time-resolved mass spectrom-

etry of tyrosine phosphorylation sites in the epidermal growth factor receptor signaling network reveals dynamic modules. Mol Cell Proteomics 4:1240–1250
10. Rush J, Moritz A, Lee KA, Guo A, Goss VL, Spek EJ, Zhang H, Zha XM, Polakiewicz RD, Comb MJ (2005) Immunoaffinity profiling of tyrosine phosphorylation in cancer cells. Nat Biotechnol 23:94–101
11. Tashiro K, Konishi H, Sano E, Nabeshi H, Yamauchi E, Taniguchi H (2006) Suppression of the ligand-mediated downregulation of epidermal growth factor receptor by Ymer, a novel tyrosine-phosphorylated and ubiquitinated protein. J Biol Chem 281:24612–24622
12. Del Castillo I, Villamar M, Moreno-Pelayo MA, del Castillo FJ, Alvarez A, Telleria D, Menendez I, Moreno F (2002) A deletion involving the connexin 30 gene in nonsyndromic hearing impairment. N Engl J Med 346:243–249
13. Kussel-Andermann P, El-Amraoui A, Safieddine S, Nouaille S, Perfettini I, Lecuit M, Cossart P, Wolfrum U, Petit C (2000) Vezatin, a novel transmembrane protein, bridges myosin VIIA to the cadherin-catenins complex. EMBO J 19:6020–6029
14. Ito M, Spicer SS, Schulte BA (1995) Cytological changes related to maturation of the organ of Corti and opening of Corti's tunnel. Hear Res 88:107–123
15. Hallworth R, McCoy M, Polan-Curtain, J (2000) Tubulin expression in the developing and adult gerbil organ of Corti. Hear Res 139:31–41
16. Pujol R, Lavigne-Rebillard M, Lenoir M (1998) Development of sensory and neural structures in the mammalian cochlea. In: Rubel EW, Popper AN, Fay RR (eds) Development of the auditory system. Springer, New York, pp 146–192
17. Belyantseva IA, Adler HJ, Curi R, Frolenkov GI, Kachar B (2000) Expression and localization of prestin and the sugar transporter GLUT-5 during development of electromotility in cochlear outer hair cells. J Neurosci 20:RC116
18. Mueller KL, Jacques BE, Kelley MW (2002) Fibroblast growth factor signaling regulates pillar cell development in the organ of corti. J Neurosci 22:9368–9377
19. Henderson CG, Tucker JB, Mogensen MM, Mackie JB, Chaplin MA, Slepecky NB, Leckie LM (1995) Three microtubule-organizing centres collaborate in a mouse cochlear epithelial cell during supracellularly coordinated control of microtubule positioning. J Cell Sci 108:37–50
20. Slepecky NB (1996) Structure of the mammalian cochlea. In: Dallos P, Popper AN, Fay RR (eds) The cochlea. Springer, New York, pp 44–129
21. Tannenbaum J, Slepecky NB (1997) Localization of microtubules containing posttranslationally modified tubulin in cochlear epithelial cells during development. Cell Motil Cytoskeleton 38:146–162
22. Sagara T, Furukawa H, Makishima K, Fujimoto S (1995) Differentiation of the rat stria vascularis. Hear Res 83:121–132
23. Forge A (1981) Ultrastructure in the stria vascularis of the guinea pig following intraperitoneal injection of ethacrynic acid. Acta Otolaryngol 92:439–457
24. Santos-Sacchi J (1982) An electronmicroscopic study of microtubules in the development of marginal cells of the mouse stria vascularis. Hear Res 6:7–13
25. Perry B, Jensen-Smith HC, Luduena RF, Hallworth R (2003) Selective expression of beta tubulin isotypes in gerbil vestibular sensory epithelia and neurons. J Assoc Res Otolaryngol 4:329–338
26. McClelland RA, Barrow D, Madden TA, Dutkowski CM, Pamment J, Knowlden JM, Gee JM, Nicholson RI (2001) Enhanced epidermal growth factor receptor signaling in MCF7 breast cancer cells after long-term culture in the presence of the pure antiestrogen ICI 182,780. Endocrinology 142:2776–2788
27. Arima T, Yamamoto T, Masuda H, Uemura T (1986) Freeze-etch visualizations of some elements in the stria vascularis. Acta Otolaryngol 102:209–215
28. Wayne S, Robertson NG, DeClau F, Chen N, Verhoeven K, Prasad S, Tranebjarg L, Morton CC, Ryan AF, Van Camp G, et al (2001) Mutations in the transcriptional activator EYA4 cause late-onset deafness at the DFNA10 locus. Hum Mol Genet 10:195–200
29. Peters LM, Anderson DW, Griffith AJ, Grundfast KM, San Agustin TB, Madeo AC, Friedman TB, Morell RJ (2002) Mutation of a transcription factor, TFCP2L3, causes progressive autosomal dominant hearing loss, DFNA28. Hum Mol Genet 11:2877–2885
30. Zine A, de Ribaupierre F (1999) Tissue-specific levels and cellular distribution of epidermal growth factor receptors within control and neomycin-damaged neonatal rat organ of Corti. J Neurobiol 38:313–322
31. Zine A, Nyffeler M, de Ribaupierre F (2000) Spatial expression patterns of epidermal growth factor receptor gene transcripts in the postnatal mammalian cochlea. Hear Res 141:19–27
32. Malgrange B, Rigo JM, Coucke P, Thiry M, Hans G, Nguyen L, van de Water TR, Moonen G, Lefebvre PP (2002) Identification of factors that maintain mammalian outer hair cells in adult organ of Corti explants. Hear Res 170:48–58
33. Doetzlhofer A, White PM, Johnson JE, Segil N, Groves AK (2004) In vitro growth and differentiation of mammalian sensory hair cell progenitors: a requirement for EGF and periotic mesenchyme. Dev Biol 272:432–447
34. Lee YW, Ozeki M, Juhn SK, Lin J (2004) Expression of platelet-derived growth factor in the developing cochlea of rats. Acta Otolaryngol 124:558–562
35. Reigstad LJ, Varhaug JE, Lillehaug JR (2005) Structural and functional specificities of PDGF-C and PDGF-D, the novel members of the platelet-derived growth factors family. FEBS J 272:5723–5741
36. James R, Bradshaw RA (1984) Polypeptide growth factors. Annu Rev Biochem 53:259–292
37. Schlessinger J (2000) Cell signalling by receptor tyrosine kinases. Cell 103:211–225
38. Pawson T, Nash P (2003) Assembly of cell regulatory systems through protein interaction domains. Science 300:445–452